

More constraints on the Georgi-Machacek model

Zahra Bairi^{1, 2, 3, *} and Amine Ahriche^{4, 5, 2, †}

¹*Laboratory of Photonic Physics and Nano-Materials,*

Department of Matter Sciences, University of Biskra, DZ-07000 Biskra, Algeria

²*Laboratoire de Physique des Particules et Physique Statistique,*

Ecole Normale Supérieure, BP 92 Vieux Kouba, DZ-16050 Algiers, Algeria

³*Department of Physics, University of M'Hamed Bougara-Boumerdes, DZ-35000 Boumerdes, Algeria.*

⁴*Department of Applied Physics and Astronomy,*

University of Sharjah, P.O. Box 27272 Sharjah, United Arab Emirates

⁵*The Abdus Salam International Centre for Theoretical Physics, Strada Costiera 11, I-34014, Trieste, Italy*

In this work, we investigate the parameter space of the Georgi-Machacek (GM) model, where we consider many theoretical and experimental constraints such as the perturbativity, vacuum stability, unitarity, electroweak precision tests, the Higgs diphoton decay, the Higgs total decay width and the LHC measurements of the signal strengths of the SM-like Higgs boson h in addition to the constraints from doubly charged Higgs bosons and Drell-Yan diphoton production and the indirect constraint from the $b \rightarrow s$ transition processes. We investigate also the possibility that the electroweak vacuum could be destabilized by unwanted wrong minima that may violate the CP and/or the electric charge symmetries. We found that about 40 % of the parameter space that fulfills the above mentioned constraints are excluded by these unwanted minima. In addition, we found that the negative searches for a heavy resonance could exclude a significant part of the viable parameter space, and future searches could exclude more regions in the parameter space.

I. INTRODUCTION

Since the discovery of a Standard Model (SM)-like 125 GeV Higgs boson at the Large Hadron Collider (LHC) [1], many questions are still open, where the SM provides no answers. For instance, the Higgs mass is found to be at the electroweak (EW) scale, while it may acquire very large radiative corrections that can reach the Planck or GUT scales within the SM. This hierarchy problem requires an unwanted fine-tuning. In addition, there are unanswered questions such as the fermions masses of difference, the origin of CP violation in the quark sector, the dark matter nature [2] and the neutrino oscillation data [3].

The discovered 125 GeV scalar has the properties of a SM-like Higgs; however, it is not known yet whether the electroweak symmetry breaking (EWSB) is triggered by one single scalar field or more. In many SM extensions, the EWSB is achieved via more than one scalar where many scalar fields acquire nonvanishing vacuum expectation values (VEVs), and the SM-like is a composite. Among these SM extensions, the so-called Georgi-Machacek (GM) model [4], where the EWSB is realized by three scalar fields. In addition to the SM doublet, the GM model includes one complex and one real scalar triplets, where a global custodial $SU(2)_V$ symmetry is preserved in the scalar potential after the EWSB. The scalar vacuum in the GM model

*Electronic address: z.bairi@univ-boumerdes.dz

†Electronic address: ahriche@sharjah.ac.ae

is defined in a way that the ρ -parameter should be within the experimentally allowed range [5],

$$\rho = \frac{g_{hWW}^{SM}}{g_{hZZ}^{SM} \cos^2 \theta_w} = 1.00039 \pm 0.00019, \quad (1)$$

with $g_{hWW}^{SM} = 2m_W^2/v$ and $g_{hZZ}^{SM} = 2m_Z^2/v$, where $v = 246.22$ GeV. This leads to a scalar spectrum with different multiplets under the global $SU(2)_V$ custodial symmetry, whose mass eigenstates give a quintet (H_5), a triplet (H_3) and two CP – *even* singlets (η and h). In our work, we consider the parameter space that corresponds to $h = h_{125}$, with $m_\eta > m_h$. One has to mention that an interesting viable parameter space exists for the case $m_\eta < m_h$, where interesting collider signatures are possible [6].

Due to the feature that the SM-like Higgs couplings to both W and Z gauge bosons could be significantly different than the SM values [7], the GM model could be phenomenologically interesting. In addition to the existence of additional CP – *odd*, singly and doubly charged scalars, the GM model could be a good benchmark for searches of beyond SM scalars; which has been extensively investigated in the literature [8]. In the decoupling limit [9], all additional beyond SM particles that are present in the GM model become heavy and the fermion and gauge bosons couplings to the SM-like Higgs boson approach the SM values. In addition to the rich phenomenology, other issues were addressed within the GM model such as the neutrino mass [10], dark matter [11], and the electroweak phase transition strength [12].

Recent measurements and negative searches at the LHC [5], such as those of the total decay width, Higgs strength modifiers and the cross section upper bounds from negative searches of new scalar resonance, could imply significant constraints on the GM model parameter space. Although the GM model includes a custodial scalar fiveplet, it has been shown that the LHC searches for the doubly charged Higgs bosons in the VBF channel $H_5^{++} \rightarrow W^+W^+$ and the Drell-Yan production of a neutral Higgs boson $pp \rightarrow H_5^0(\gamma\gamma)H^+$ impose interesting bounds on the parameter space [13], as well as the indirect constraints from the $b \rightarrow s$ transition processes that exclude all the benchmark points (BPs) with large v_ξ [14]. In addition, the GM scalar potential structure may admit many minima beside the electroweak (EW) vacuum that could break the electric charge and/or the CP symmetry spontaneously. In case where such minima exist, they should not be deeper than the EW vacuum, which may affect the parameter space that is in agreement with the previously mentioned constraints. In [15], the authors performed a global fit analysis for the GM model free parameter and obtained some limits on the mixing angles and the heavy new scalar masses and decay widths. However, since the constraints from the $b \rightarrow s$ transition processes were considered in [15]; and the LHC measurements used to constrain the GM model have been significantly updated, an analysis for the full model parameter space is required. Here, we aim to investigate the impact of all the relevant constraints on the model by performing a full numerical scan over the whole parameter space.

In this work, we give a brief introduction of the GM model in Sec II, where the scalar potential and the mass spectrum are described. In Sec III, we discuss the possible existence of new minima that could be deeper than the EW vacuum. Then, after categorizing these unwanted minima according to the preserved/broken (CP and electric charge) symmetries, one considers the EW vacuum to be the deepest one as a novel constraint on the GM model. In Sec IV, we discuss different theoretical and experimental constraints on the model such as the unitarity, vacuum stability, the total Higgs decay width and signal strength modifiers, the electroweak precision tests, and the diphoton Higgs decay. In addition, we consider the recent ATLAS and CMS constraints on the heavy CP – *even* scalar η and from the negative searches for the doubly charged Higgs bosons in the VBF channel $H_5^{++} \rightarrow W^+W^+$, and the Drell-Yan production of a neutral Higgs boson $pp \rightarrow H_5^0(\gamma\gamma)H^+$. We show our numerical results and discussion in Sec V, and our conclusion in Sec VI.

II. THE MODEL: PARAMETERS AND MASS SPECTRUM

In the GM model, the scalar sector consists of a scalar doublet $(\phi^+, \phi^0)^T$ with hypercharge $Y = 1$, and two triplet representations $(\chi^{++}, \chi^+, \chi^0)^T$ and $(\xi^+, \xi^0, -\xi^-)^T$ with hypercharge $Y = 2, 0$, respectively. These representations can be written as

$$\Phi = \begin{pmatrix} \phi^{0*} & \phi^+ \\ -\phi^{+*} & \phi^0 \end{pmatrix}, \quad \Delta = \begin{pmatrix} \chi^{0*} & \xi^+ & \chi^{++} \\ -\chi^{+*} & \xi^0 & \chi^+ \\ \chi^{++*} & -\xi^{+*} & \chi^0 \end{pmatrix}, \quad (2)$$

where $\phi^- = \phi^{+*}$, $\xi^- = \xi^{+*}$, $\chi^{--} = \chi^{++*}$, $\chi^- = \chi^{+*}$. The neutral components in (2) can be expressed by

$$\phi^0 = \frac{1}{\sqrt{2}}(v_\phi + h_\phi + ia_\phi), \quad \chi^0 = \frac{1}{\sqrt{2}}(v_\chi + h_\chi + ia_\chi), \quad \xi^0 = v_\xi + h_\xi, \quad (3)$$

where v_ϕ , v_χ and v_ξ are the VEVs for ϕ^0 , χ^0 and ξ^0 , respectively. Here, we have three *CP* – *even* scalar degrees of freedom (d.o.f.) $\{h_\phi, h_\chi, h_\xi\}$, two *CP* – *odd* d.o.f. $\{a_\phi, a_\chi\}$, six singly charged d.o.f. $\{\phi^\pm, \chi^\pm, \xi^\pm\}$ and two doubly charged d.o.f. $\chi^{\pm\pm}$. The most general scalar potential invariant under the global symmetry $SU(2)_L \times SU(2)_R \times U(1)_Y$ is given by

$$\begin{aligned} V(\Phi, \Delta) = & \frac{m_1^2}{2} \text{Tr}[\Phi^\dagger \Phi] + \frac{m_2^2}{2} \text{Tr}[\Delta^\dagger \Delta] + \lambda_1 (\text{Tr}[\Phi^\dagger \Phi])^2 + \lambda_2 \text{Tr}[\Phi^\dagger \Phi] \text{Tr}[\Delta^\dagger \Delta] \\ & + \lambda_3 \text{Tr}[(\Delta^\dagger \Delta)^2] + \lambda_4 (\text{Tr}[\Delta^\dagger \Delta])^2 - \lambda_5 \text{Tr}[\Phi^\dagger \frac{\sigma^a}{2} \Phi \frac{\sigma^b}{2}] \text{Tr}[\Delta^\dagger T^a \Delta T^b] \\ & - \mu_1 \text{Tr}[\Phi^\dagger \frac{\sigma^a}{2} \Phi \frac{\sigma^b}{2}] (U \Delta U^\dagger)_{ab} - \mu_2 \text{Tr}[\Delta^\dagger T^a \Delta T^b] (U \Delta U^\dagger)_{ab}, \end{aligned} \quad (4)$$

with $\sigma^{1,2,3}$ are the Pauli matrices and $T^{1,2,3}$ correspond to the generators of the $SU(2)$ triplet representation, that are given by

$$T^1 = \frac{1}{\sqrt{2}} \begin{pmatrix} 0 & 1 & 0 \\ 1 & 0 & 1 \\ 0 & 1 & 0 \end{pmatrix}, \quad T^2 = \frac{1}{\sqrt{2}} \begin{pmatrix} 0 & -i & 0 \\ i & 0 & -i \\ 0 & i & 0 \end{pmatrix}, \quad T^3 = \begin{pmatrix} 1 & 0 & 0 \\ 0 & 0 & 0 \\ 0 & 0 & -1 \end{pmatrix}, \quad (5)$$

and the matrix U is defined as

$$U = \frac{1}{\sqrt{2}} \begin{pmatrix} -1 & 0 & 1 \\ -i & 0 & -i \\ 0 & \sqrt{2} & 0 \end{pmatrix}. \quad (6)$$

The custodial symmetry condition at tree-level $m_W^2 = m_Z^2 \cos^2 \theta_W$ implies $v_\chi = \sqrt{2}v_\xi$ and $v_\phi^2 + 8v_\xi^2 \equiv v^2 = (246.22 \text{ GeV})^2$, where m_W , m_Z and θ_W are the gauge bosons masses and the Weinberg mixing angle. It would be useful to introduce the parameter $t_\beta \equiv \tan \beta = 2\sqrt{2}v_\xi/v_\phi$ to describe the relations between the VEV's. By using the tadpole conditions, one can eliminate the parameters $m_{1,2}^2$ as

$$\begin{aligned} m_1^2 = & -4\lambda_1 c_\beta^2 v^2 + \frac{3}{8}(-2\lambda_2 + \lambda_5) s_\beta^2 v^2 + \frac{3}{4\sqrt{2}} \mu_1 s_\beta v, \\ m_2^2 = & (-2\lambda_2 + \lambda_5) c_\beta^2 v^2 - \frac{1}{2}(\lambda_3 + 3\lambda_4) s_\beta^2 v^2 + \frac{\mu_1}{\sqrt{2}} \frac{c_\beta^2 v}{s_\beta} + \frac{3}{\sqrt{2}} \mu_2 s_\beta v. \end{aligned} \quad (7)$$

After the EWSB, the Goldstone bosons are eaten by the massive W and Z bosons, and we are left with the following mass eigenstates: three CP – *even* eigenstates $\{h, \eta, H_5^0\}$, one CP – *odd* eigenstate H_3^0 , two singly charged scalars $\{H_3^\pm, H_5^\pm\}$, and one doubly charged scalar $H_5^{\pm\pm}$,

$$h = c_\alpha h_\phi - \frac{s_\alpha}{\sqrt{3}}(\sqrt{2}h_\chi + h_\xi), \quad \eta = s_\alpha h_\phi + \frac{c_\alpha}{\sqrt{3}}(\sqrt{2}h_\chi + h_\xi), \quad H_5^0 = \sqrt{\frac{2}{3}}h_\xi - \sqrt{\frac{1}{3}}h_\chi, \\ H_3^0 = -s_\beta a_\phi + c_\beta a_\chi, \quad H_3^\pm = -s_\beta \phi^\pm + c_\beta \frac{1}{\sqrt{2}}(\chi^\pm + \xi^\pm), \quad H_5^\pm = \frac{1}{\sqrt{2}}(\chi^\pm - \xi^\pm), \quad H_5^{\pm\pm} = \chi^{\pm\pm}. \quad (8)$$

The mixing angle α of the CP – *even* sector can be defined by $\tan 2\alpha = 2M_{12}^2/(M_{22}^2 - M_{11}^2)$, where M^2 is the mass squared matrix in the basis $\{h_\phi, \sqrt{\frac{2}{3}}h_\chi + \frac{1}{\sqrt{3}}h_\xi\}$, whose elements are given by

$$M_{11}^2 = 8\lambda_1 c_\beta^2 v^2, \\ M_{12}^2 = \frac{\sqrt{3}}{2}c_\beta v[-\mu_1 + \sqrt{2}(2\lambda_2 - \lambda_5)s_\beta v], \\ M_{22}^2 = \frac{\mu_1}{\sqrt{2}}\frac{c_\beta^2 v}{s_\beta} - \frac{3}{\sqrt{2}}\mu_2 s_\beta v + (\lambda_3 + 3\lambda_4)s_\beta^2 v^2. \quad (9)$$

This allows us to write the SM-like Higgs bosons and the heavy scalar (η) eigenmasses as $m_{h,\eta}^2 = \frac{1}{2}[M_{11}^2 + M_{22}^2 \mp \sqrt{(M_{11}^2 - M_{22}^2)^2 + 4(M_{12}^2)^2}]$. The other eigenmasses are

$$m_{H_3^0}^2 = m_{H_3^\pm}^2 = m_3^2 = \left(\frac{\mu_1}{\sqrt{2}s_\beta} + \frac{\lambda_5}{2}\right)v^2, \\ m_{H_5^0}^2 = m_{H_5^\pm}^2 = m_{H_5^{\pm\pm}}^2 = m_5^2 = \frac{\mu_1}{\sqrt{2}}\frac{c_\beta^2 v}{s_\beta} + \frac{6}{\sqrt{2}}\mu_2 s_\beta v + \frac{3}{2}\lambda_5 c_\beta^2 v^2 + \lambda_3 s_\beta^2 v^2. \quad (10)$$

Since, we will take the masses as input parameters, the quartic couplings λ 's can be expressed as

$$\lambda_1 = \frac{\varrho_1 c_\alpha^2 + \varrho_2 s_\alpha^2}{8v^2 c_\beta^2}, \quad \lambda_2 = -\frac{c_\alpha s_\alpha (\varrho_1 - \varrho_2)}{\sqrt{6}v^2 c_\beta s_\beta} + \frac{m_3^2}{v^2} - \frac{\mu_1}{2\sqrt{2}v s_\beta}, \\ \lambda_3 = -\frac{3c_\beta^2 m_3^2}{s_\beta^2 v^2} + \frac{m_5^2}{s_\beta^2 v^2} + \frac{\sqrt{2}(\mu_1 c_\beta^2 - 3\mu_2 s_\beta^2)}{s_\beta^3 v}, \quad \lambda_5 = \frac{2m_3^2}{v^2} - \frac{\sqrt{2}\mu_1}{v s_\beta}, \\ \lambda_4 = \frac{\varrho_1 s_\alpha^2 + \varrho_2 c_\alpha^2}{3s_\beta^2 v^2} + \frac{c_\beta^2 m_3^2}{s_\beta^2 v^2} - \frac{m_5^2}{3s_\beta^2 v^2} - \frac{\mu_1 c_\beta^2 - 3\mu_2 s_\beta^2}{\sqrt{2}s_\beta^3 v}, \quad (11)$$

with $\varrho_1 = \min(m_h^2, m_\eta^2)$ and $\varrho_2 = \max(m_h^2, m_\eta^2)$. The formulas of $\lambda_{1,2,4}$ here are valid for both cases of $m_h < m_\eta$ and $m_h > m_\eta$.

III. AVOIDING WRONG MINIMA

Since the scalar potential is a function of different fields; three CP – *even*, two CP – *odd* and eight charged scalars, the possibility of other existing minima that are different and deeper than $(\Re(\phi^0), \Re(\chi^0), \Re(\xi^0)) = (v_\phi, \sqrt{2}v_\xi, v_\xi)$ would destabilize the EW vacuum. In [9, 16], the authors adopted a simplified field parametrization to investigate the vacuum stability and the boundness from below conditions, where the scalar potential (4) can be written as

$$V = \frac{1}{2} \frac{r^2}{(1 + \tan^2 \gamma)} [m_1^2 + m_2^2 \tan^2 \gamma] + \frac{r^3}{(1 + \tan^2 \gamma)^{3/2}} \tan \gamma [-\sigma\mu_1 - \rho\mu_2 \tan^2 \gamma] \\ + \frac{r^4}{(1 + \tan^2 \gamma)^2} [\lambda_1 + (\lambda_2 - \omega\lambda_5) \tan^2 \gamma + (\zeta\lambda_3 + \lambda_4) \tan^4 \gamma], \quad (12)$$

with

$$\begin{aligned}
r &= \sqrt{\text{Tr}(\Phi^\dagger \Phi) + \text{Tr}(\Delta^\dagger \Delta)}, \quad \text{Tr}(\Phi^\dagger \Phi) = r^2 \cos^2 \gamma, \quad \text{Tr}(\Delta^\dagger \Delta) = r^2 \sin^2 \gamma, \\
\text{Tr}(\Delta^\dagger \Delta \Delta^\dagger \Delta) &= \zeta r^4 \sin^4 \gamma, \quad \text{Tr}(\Phi^\dagger \sigma^a \Phi \sigma^b) \text{Tr}(\Delta^\dagger T^a \Delta T^b) = \omega r^4 \cos^2 \gamma, \quad \sin^2 \gamma, \\
\text{Tr}(\Phi^\dagger \sigma^a \Phi \sigma^b) (U \Delta U^\dagger)_{ab} &= \sigma r^3 \sin \gamma \cos^2 \gamma, \quad \text{Tr}(\Delta^\dagger T^a \Delta T^b) (U \Delta U^\dagger)_{ab} = \rho r^3 \sin^3 \gamma, \\
r &\in [1, \infty[, \gamma \in [0, \frac{\pi}{2}], \zeta \in [\frac{1}{3}, 1], \omega \in [-\frac{1}{4}, \frac{1}{2}], \sigma \in [-\frac{\sqrt{3}}{4}, \frac{\sqrt{3}}{4}], \rho \in [-\frac{2}{\sqrt{3}}, \frac{2}{\sqrt{3}}].
\end{aligned} \tag{13}$$

For instance, the conditions for the boundness from below of the scalar potential can be ensured by imposing the coefficients of the quartic term i.e., the second line in (12) to be positive, which leads to

$$\lambda_1 > 0, \quad \zeta \lambda_3 + \lambda_4 > 0, \quad \lambda_2 - \omega \lambda_5 + 2\sqrt{\lambda_1(\zeta \lambda_3 + \lambda_4)} > 0. \tag{14}$$

The parametrization (12) reduces the searches for the potential minima into looking for specific sets of the parameters values in the ranges (13) that make (12) minimal. Here, we will not adopt this approach due to many reasons, among them the fact that the parameters in (13) are not fully independent. In other words, any field configuration in the field space can be defined by a single set of the parameters in (13), while any parameters set in (13) does not necessarily correspond to a well-defined field configuration. In addition, when a field configuration corresponds to a minimum, it does not show whether it preserves or violates the CP symmetry and/or the electric charge.

The scalar potential includes 13 scalar d.o.f.: three $CP - even$, two $CP - odd$, six singly charged and two doubly charged. The scalar potential must respect the electric charge conservation by demanding (1) either the VEVs of all charged scalars to be vanishing, i.e., $\langle \phi^\pm \rangle = \langle \chi^\pm \rangle = \langle \xi^\pm \rangle = \langle \chi^{++} \rangle = 0$, or (2) any existing electric charge breaking minimum should not be deeper than the EW one. The CP symmetry could be spontaneously violated when some of the $CP - odd$ fields acquire a VEV, i.e., $\langle \Im(\phi^0) \rangle, \langle \Im(\chi^0) \rangle \neq 0$, where this case is experimentally allowed within the data from ACME Collaboration on the electron and neutron electric dipole moment (EDM) [17]. In the case where both CP symmetry and the electric charge are conserved, other minima beside the EW vacuum ($\Re(\phi^0), \Re(\chi^0), \Re(\xi^0) = (v_\phi, \sqrt{2}v_\xi, v_\xi)$), could exist. In order to ensure the EW vacuum stability, we need to check that the scalar potential at ($\Re(\phi^0), \Re(\chi^0), \Re(\xi^0) = (v_\phi, \sqrt{2}v_\xi, v_\xi)$) is the true global minimum. Then, in our work we consider only the parameter space where the EW vacuum is deeper than an any other existing minimum whether it preserves or violates the CP and/or electric charge symmetries.

Then, finding these wrong minima requires the minimization of the potential (4) along all the $CP - even$, $CP - odd$ and the charged fields directions is mandatory. As the minimization along the $CP - odd$ 2D space $\{\Im(\phi^0), \Im(\chi^0)\}$ is straightforward, it requires along the charged directions a useful parametrization for the charged fields. This can be done either by writing both singly and doubly charged fields as $X^\pm = \frac{1}{\sqrt{2}}(x_1 \pm ix_2)$ [18], or adopting the parametrization $X^\pm = |X|e^{\pm i\varrho}$. In [18], the authors studied the vacuum stability of a Z_2 symmetric version of the GM model, where the cubic terms of the scalar potential are absent. They used the parametrization $X^\pm = \frac{1}{\sqrt{2}}(x_1 \pm ix_2)$ to investigate special cases in which CP and/or electric charge symmetries could be violated. However, this study is not applicable to our research due to the global Z_2 symmetry (i.e., $\mu_1 = \mu_2 = 0$), which renders the possible vacua drastically different from the standard case where μ_1 and μ_2 are nonzero.

In our work, we consider the polar parametrization where the minimization conditions are $\partial V / \partial X = \partial V / \partial \varrho = 0$ at the charge breaking vacuum. Although in the $CP - even$ directions, there may exist other

minima beside the EW one that could be deeper. Therefore, one has to search for all minima along all directions (CP – even, CP – odd and charged) and check that they are not deeper than the EW vacuum $(v_\phi, \sqrt{2}v_\xi, v_\xi)$.

After a careful analysis, we found eight minima in the CP – even directions $\{h_\phi, h_\chi, h_\xi\}$, three minima along the CP – odd directions $\{a_\phi, a_\chi\}$, eight minima along the singlet charged fields directions $\{\phi^\pm, \chi^\pm, \xi^\pm\}$, and a minimum along the doubly charged direction $\chi^{\pm\pm}$. We denote the potential values at these wrong minima by $V_{i=1,8}^{0+}$, $V_{i=1,3}^{0-}$, $V_{i=1,8}^\pm$ and V^\pm , respectively, and we give their coordinates in Appendix C. Getting the analytical formula for the CP -conserving and electric charge violating minima given in (C1), (C2) and (C3) was an easy task since they were special cases of one or two-dimensional problem. Indeed, there could be other minima defined in 3D, which will be defined numerically.

Then, the EW vacuum should be deeper than all these local minima, i.e.,

$$V(\mathfrak{R}(\phi^0)) = v_\phi, \mathfrak{R}(\chi^0) = \sqrt{2}v_\xi, \mathfrak{R}(\xi^0) = v_\xi < \min\{V_i^{0+}, V_i^{0-}, V_i^\pm, V^{\pm\pm}, 0\}, \quad (15)$$

where the zero in the last position represents the obviously wrong vacuum $V(0, 0, 0)$. As we will see later, the condition (15) could exclude more than 40 % of the parameter space.

IV. THEORETICAL AND EXPERIMENTAL CONSTRAINTS

In what follows, we discuss different theoretical and experimental constraints on the GM model that are related to many aspects such as the vacuum stability, unitarity, the Higgs decays, the electroweak precision tests, in addition to the constraints from negative searches for heavy scalar resonances at the LHC.

Tree-level unitarity

The bound from perturbative unitarity is obtained by requiring the zeroth partial wave amplitude for any elastic $2 \rightarrow 2$ bosonic scatterings does not become too large to violate S matrix unitarity. In the high CM energy regime, the gauge fields can be replaced by their corresponding Goldstone scalars. This means that the amplitude, a_0 satisfy $|a_0| \leq 1$ or $|Re a_0| \leq 1/2$. Then, the perturbative unitarity bounds in the GM model reads [9]

$$\begin{aligned} \sqrt{(6\lambda_1 - 7\lambda_3 - 11\lambda_4)^2 + 36\lambda_2^2} + |6\lambda_1 + 7\lambda_3 + 11\lambda_4| < 4\pi, \quad |2\lambda_3 + \lambda_4| < \pi, \\ \sqrt{(2\lambda_1 + \lambda_3 - 2\lambda_4)^2 + \lambda_5^2} + |2\lambda_1 - \lambda_3 + 2\lambda_4| < 4\pi, \quad |\lambda_2 - \lambda_5| < 2\pi. \end{aligned} \quad (16)$$

Boundness from below

To ensure the scalar potential boundness from below condition, the coefficients of the quartic term along any direction in the fields space must be positive. This leads to the conditions [19]

$$\begin{aligned} \lambda_1 > 0, \lambda_4 > \begin{cases} -\frac{1}{3}\lambda_3 & \text{for } \lambda_3 \geq 0, \\ -\lambda_3 & \text{for } \lambda_3 < 0, \end{cases}, \\ \lambda_2 > \begin{cases} \frac{1}{2}\lambda_5 - 2\sqrt{\lambda_1(\frac{1}{3}\lambda_3 + \lambda_4)} & \text{for } \lambda_5 \geq 0 \text{ and } \lambda_3 \geq 0, \\ \omega_+(\zeta)\lambda_5 - 2\sqrt{\lambda_1(\zeta\lambda_3 + \lambda_4)} & \text{for } \lambda_5 \geq 0 \text{ and } \lambda_3 < 0, \\ \omega_-(\zeta)\lambda_5 - 2\sqrt{\lambda_1(\zeta\lambda_3 + \lambda_4)} & \text{for } \lambda_5 < 0, \end{cases} \end{aligned} \quad (17)$$

where

$$\omega \pm (\zeta) = \frac{1}{6}(1 - B) \pm \frac{\sqrt{2}}{3}[(1 - B)(\frac{1}{2} + B)]^{1/2}, \quad B \equiv \sqrt{\frac{3}{2} \left(\zeta - \frac{1}{3} \right)} \in [0, 1]. \quad (18)$$

The last two conditions for λ_2 must be satisfied for all values of $\zeta \in [\frac{1}{3}, 1]$. Numerically, we consider 1000 steps in the interval of ζ .

The Higgs boson decays

In this setup, the SM-like Higgs boson h (the scalar with the mass $m_h = 125.25$ GeV) decays mainly into the fermions pairs $\tau^+\tau^-$, $c\bar{c}$, $b\bar{b}$ and the gauge bosons WW^* and ZZ^* . The partial decay width of the channel $h \rightarrow XX$ can be parametrized as $\Gamma(h \rightarrow XX) = \kappa_X^2 \Gamma^{SM}(h \rightarrow XX)$, where the coefficients,

$$\kappa_F = \frac{g_{hff}^{GM}}{g_{hff}^{SM}} = \frac{c_\alpha}{c_\beta}, \quad \kappa_V = \frac{g_{hVV}^{GM}}{g_{hVV}^{SM}} = c_\alpha c_\beta - \sqrt{\frac{8}{3}} s_\alpha s_\beta, \quad (19)$$

represent the Higgs couplings modifiers with respect to the SM. This allows us to write the total Higgs decay width as

$$\Gamma_h^{tot} = \Gamma_h^{SM} \sum_{X=SM} \kappa_X^2 \mathcal{B}^{SM}(h \rightarrow XX), \quad (20)$$

where $\Gamma_h^{SM} = 4.08$ MeV [5] and $\mathcal{B}^{SM}(h \rightarrow XX)$ are the SM values for total decay width and the branching ratios for the Higgs boson, respectively. Here, other decay channels like $h \rightarrow H_3 H_3 / H_5 H_5$ could not be open due to the constraints on the charged scalar masses $m_{H_3^\pm}^2$, $m_{H_5^\pm}^2$ and $m_{H_5^{\pm\pm}}^2$. The GM value for the Higgs boson (20) should lie in the range [20],

$$2.1 \text{ MeV} < \Gamma_h^{tot} < 7.2 \text{ MeV}. \quad (21)$$

The signal strengths of the SM-like Higgs boson h have been measured in the LHC in various channels, where significant constraints are established [5]. Here, one can translate these constraints on the partial signal strength modifiers into bounds on the GM Higgs couplings modifiers κ_X . In our analysis, we consider only the gluon-gluon fusion (ggF) Higgs production channel, where the partial Higgs signal strength modifier of the channel $h \rightarrow XX$ can be simplified as

$$\mu_{XX} = \frac{\sigma(pp \rightarrow h) \times \mathcal{B}(h \rightarrow XX)}{\sigma^{SM}(pp \rightarrow h) \times \mathcal{B}^{SM}(h \rightarrow XX)} = \kappa_F^2 \kappa_X^2 \frac{\Gamma_h^{SM}}{\Gamma_h^{tot}}, \quad (22)$$

with $\sigma(gg \rightarrow h) [\sigma^{SM}(gg \rightarrow h)]$ is the ggF production cross section in the GM [SM] model. The constraints on the invisible and undetermined channel are irrelevant here since they are closed due to the scalar masses $m_{3,5} > 78$ GeV, so $\mathcal{B}(h \rightarrow H_3^\pm H_3^\mp, H_5^\pm H_5^\mp) = 0$. This means that the experimental measurements of (22) will constraint significantly the coefficients (19). Here, we consider the allowed values from all partial Higgs strength modifiers within a 3σ range. The very recent 1σ values are given in PDG by [5]

$$\begin{aligned} \mu_{WW} &= 1.19 \pm 0.12, \quad \mu_{ZZ} = 1.01 \pm 0.07, \quad \mu_{b\bar{b}} = 0.98 \pm 0.12, \\ \mu_{\mu^+\mu^-} &= 1.19 \pm 0.34, \quad \mu_{\tau^+\tau^-} = 1.15_{-0.15}^{+0.16}. \end{aligned} \quad (23)$$

It is expected that (23) put severe bounds on the Higgs coupling modifiers $\kappa_{F,V}$, and consequently the mixing angles α and β .

The electroweak precision tests

The structure of the scalar-gauge interactions in the GM model makes the constraints from the EWPTs very important. In the GM model, the T parameter estimation is problematic since it is divergent, but the S and U parameters are calculable. Since the absolute value of the U parameter is found to be very small < 0.01 , we will consider the constraint from the S parameter by fixing the $U = 0$. The experimental values for the oblique parameter S is extracted for the SM Higgs mass $m_h = 125.25$ GeV, where we consider the 2σ range in our numerical scan $S = 0.05 \pm 0.11$ [22]. The new contributions to the S parameter [14] in the GM model are given by

$$\begin{aligned} \Delta S = S_{GM} - S_{SM} = & \frac{s_W^2 c_W^2}{e^2 \pi} \left\{ -\frac{e^2}{12 s_W^2 c_W^2} (\log m_3^2 + 5 \log m_5^2) + 2 \left| g_{ZhH_3^0} \right|^2 f_1(m_h, m_3) \right. \\ & + 2 \left| g_{Z\eta H_3^0} \right|^2 f_1(m_\eta, m_3) + 2 \left(\left| g_{ZH_5^0 H_3^0} \right|^2 + 2 \left| g_{ZH_5^+ H_5^-} \right|^2 \right) f_1(m_5, m_3) + \left| g_{ZZh} \right|^2 \left[\frac{f_1(m_Z, m_h)}{2m_Z^2} - f_3(m_Z, m_h) \right] \\ & - \left| g_{ZZh}^{SM} \right|^2 \left[\frac{f_1(m_Z, m_h^{SM})}{2m_Z^2} - f_3(m_Z, m_h^{SM}) \right] + \left| g_{ZZ\eta} \right|^2 \left[\frac{f_1(m_Z, m_\eta)}{2m_Z^2} - f_3(m_Z, m_\eta) \right] \\ & \left. + \left| g_{ZZH_5^0} \right|^2 \left[\frac{f_1(m_Z, m_5)}{2m_Z^2} - f_3(m_Z, m_5) \right] + 2 \left| g_{ZW^+ H_5^-} \right|^2 \left[\frac{f_1(m_W, m_5)}{2m_W^2} - f_3(m_W, m_5) \right] \right\}, \quad (24) \end{aligned}$$

with the functions $f_{1,3}$ and the couplings g_{ZXY} are given in Appendixes A and B, respectively.

The Higgs decays $h \rightarrow \gamma\gamma, \gamma Z$

The Higgs decay into two photons or a photon and a Z gauge boson are induced through a loop of charged particles. To estimate any new physics effect on these Higgs decays, the ratios $R_{\gamma\gamma, \gamma Z} = \mathcal{B}(h \rightarrow \gamma\gamma, \gamma Z) / \mathcal{B}^{SM}(h \rightarrow \gamma\gamma, \gamma Z)$ are estimated and used to constrain the charged scalar masses and their couplings to the Higgs boson. According to the latest data, we have $R_{\gamma\gamma} = 1.10 \pm 0.07$ [5]. According to the Feynman diagrams in Fig. 1, the deviation of $R_{\gamma\gamma}$ from unity, may come from many vertices such as $\tilde{g}\tilde{g}h$, $t\bar{t}h$ and W^+W^-h as well due to new vertices involving new charged scalars.

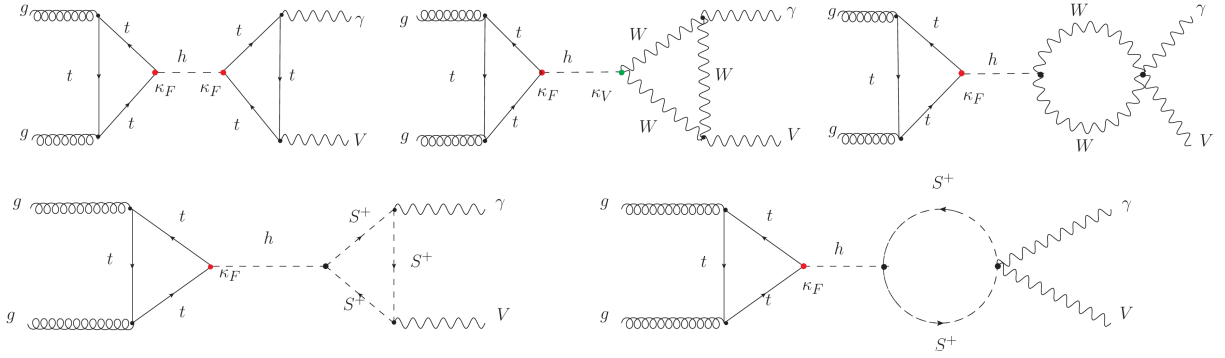


FIG. 1: Feynman diagrams relevant to the Higgs decay $h \rightarrow \gamma V$ ($V = \gamma, Z$) at the LHC. The red and blue points refer to the vertices that could be modified with respect to the SM by the factors κ_F and κ_V , respectively.

From the diagrams in Fig. 1, one finds the ratios

$$R_{\gamma\gamma} = \kappa_F^2 \left| \frac{\frac{v}{2} \sum_X \frac{g_{hXX}}{m_X^2} Q_X^2 A_0^{\gamma\gamma}(\tau_X) + \kappa_V A_1^{\gamma\gamma}(\tau_W) + \kappa_F \frac{4}{3} A_{1/2}^{\gamma\gamma}(\tau_t)}{A_1^{\gamma\gamma}(\tau_W) + \frac{4}{3} A_{1/2}^{\gamma\gamma}(\tau_t)} \right|^2, \quad (25)$$

$$R_{\gamma Z} = \kappa_F^2 \left| \frac{v \sum_X \frac{g_{hXX} C_{ZZXX}}{m_X^2} Q_X A_0^{\gamma Z}(\tau_X, \lambda_X) + \kappa_V A_1^{\gamma Z}(\tau_W, \lambda_W) + \kappa_F \frac{-6+16s_w^2}{3s_w c_w} A_{1/2}^{\gamma Z}(\tau_t, \lambda_t)}{A_1^{\gamma Z}(\tau_W, \lambda_W) + \frac{-6+16s_w^2}{3s_w c_w} A_{1/2}^{\gamma Z}(\tau_t, \lambda_t)} \right|^2, \quad (26)$$

where $X = H_3^+, H_5^+, H_5^{++}$ stands for all charged scalars inside the loop diagrams, Q_X is the electric charge of the field X in units of $|e|$, $\tau_X = 4m_X^2/m_h^2$, $\lambda_X = 4m_X^2/m_Z^2$; and the functions $A_i^{\gamma\gamma, \gamma Z}$ and coefficients g_{hXX} and C_{ZZXX} are given in Appendixes A and B, respectively.

Constraints from the production/decay of the heavy scalar η

After the discovery of the Higgs boson with $m_h = 125.25$ GeV, efforts have been devoted to search for heavy neutral scalar boson through different channels over a wide mass range. Such results can also be used to impose constraints on models with many neutral scalars such as the GM model.

The two CP – *even* eigenstates h and η are defined through a mixing angle α and ($m_h < m_\eta$), where the light eigenstate h is identified to be the SM-like Higgs boson with the measured mass $m_h = 125.25$ GeV. Here, the heavy scalar η has similar couplings as the SM Higgs boson, but modified with the factors,

$$\zeta_V = \frac{g_{\eta VV}^{GM}}{g_{hVV}^{SM}} = s_\alpha c_\beta + \sqrt{\frac{8}{3}} c_\alpha s_\beta, \quad \zeta_F = \frac{g_{\eta FF}^{GM}}{g_{hFF}^{SM}} = \frac{s_\alpha}{c_\beta}. \quad (27)$$

The partial decay width of the heavy scalar η into SM final states can be written as $\Gamma(\eta \rightarrow X\bar{X}) = \zeta_X^2 \Gamma^{SM}(\eta \rightarrow X\bar{X})$, where $\Gamma^{SM}(\eta \rightarrow X\bar{X})$ is the Higgs partial decay width estimated at $m_h \rightarrow m_\eta$ [23]. In addition, there exist other BSM decay channels like $\eta \rightarrow hh, H_3 H_3, H_5 H_5$ when kinematically allowed. The partial decay width for these channels is given by

$$\Gamma(\eta \rightarrow Y\bar{Y}) = r_Y \frac{|g_{\eta Y\bar{Y}}|^2}{32\pi m_\eta} \sqrt{1 - 4 \frac{m_Y^2}{m_\eta^2}}, \quad (28)$$

with $Y = h, H_3^0, H_3^\pm, H_5^0, H_5^\pm, H_5^{\pm\pm}$, $r_{h, H_3^0, H_5^0} = 1$ and $r_{H_3^\pm, H_5^\pm, H_5^{\pm\pm}} = 2$. Then, the heavy scalar η total decay width can be written as

$$\Gamma_\eta^{tot} = \sum_{Y \neq SM} \Gamma(\eta \rightarrow Y\bar{Y}) + \Gamma_\eta^{SM} \sum_{X=SM} \zeta_X^2 \mathcal{B}^{SM}(\eta \rightarrow X\bar{X}), \quad (29)$$

where Γ_η^{SM} and $\mathcal{B}^{SM}(\eta \rightarrow X\bar{X})$ are the Higgs total decay width and branching ratios estimated at $m_h \rightarrow m_\eta$ [23]. Since the heavy scalar η decays into all SM final states, it can be searched at the LHC via the processes: (1) $pp \rightarrow \eta \rightarrow \ell\ell, jj, VV$ and $pp \rightarrow \eta \rightarrow hh$. For the first type, we include the recent ATLAS analysis at 13 TeV with 139 fb^{-1} $pp \rightarrow \eta \rightarrow \tau\tau$ [24] and $pp \rightarrow S \rightarrow ZZ$ via the channels $llll$ and $ll\nu\nu$ [25]. In the other side, when checking the bounds from the decay $pp \rightarrow \eta \rightarrow WW$, one finds that the recent CMS analyses [26] are not convenient to use here, due to the considered large mass range ($m_\eta > 1$ TeV) in the analysis. For the second type, we use the recent ATLAS combination [27] that includes the analyses at 13 TeV with 139 fb^{-1} via the channels $hh \rightarrow b\bar{b}\tau\tau$ [28], $hh \rightarrow b\bar{b}b\bar{b}$ [29] and $hh \rightarrow b\bar{b}\gamma\gamma$ [30].

Here, we can take all the above mentioned analyses to constrain the GM model parameters that are relevant to the heavy scalar η . We define the cross section of the Heavy scalar η in function of the branching

ratios and decay width as

$$\sigma(pp \rightarrow \eta) \times \mathcal{B}(\eta \rightarrow X\bar{X}) = \zeta_F^2 \zeta_X^2 \frac{\Gamma_{SM}^{tot}(\eta)}{\Gamma^{tot}(\eta)} \sigma^{SM}(pp \rightarrow \eta) \times \mathcal{B}^{SM}(\eta \rightarrow X\bar{X}), \quad (30)$$

where $\mathcal{B}^{SM}(\eta \rightarrow X\bar{X})$ are the branching ratios of the heavy scalar η decaying into a pair of gauge bosons or fermions via the ggF production mode of η , $\sigma(pp \rightarrow \eta)$ and $\sigma^{SM}(pp \rightarrow \eta)$ are the proton-proton collision production cross section.

LHC Constraints on the triplet and fiveplet Scalars

Here, we implement some of the most stringent constraints, especially the vector boson fusion (VBF) production of H_5^{++} and the Drell-Yan production of a neutral Higgs boson.

A. VBF $H_5^{++} \rightarrow W^+W^+ \rightarrow$ like sign dileptons

The experimental bound on s_H as a function of m_5 is constrained by a CMS result of 35.9 fb^{-1} of LHC run 2 (13 TeV) data [31] for $m_5 > 200 \text{ GeV}$, we assume that the signal production cross section is proportional to s_H^2 where

$$(s_H^{limit})^2 \times \mathcal{B}(H_5^{++} \rightarrow W^+W^+) = (s_H^{CMS})^2, \quad (31)$$

with $(s_H^{CMS})^2$ is the bound presented at [31] that corresponds to $\mathcal{B}(H_5^{++} \rightarrow W^+W^+) = 1$.

B. Drell-Yan $H_5^0 H_5^\pm$ with $H_5^0 \rightarrow \gamma\gamma$

Concerning the Drell-Yan production of $H_5^0 H_5^\pm$ with H_5^0 , there exist two ATLAS searches for diphoton resonances in the mass range $65 < m_5 < 600 \text{ GeV}$ using 20.3 fb^{-1} of LHC run 1 (8 TeV) data [32] and of the 36.7 fb^{-1} luminosity of LHC run 2 (13 TeV) data in the mass range $200 < m_5 < 2700 \text{ GeV}$ [33]. The total cross sections at 8 TeV and 13 TeV for $H_5^0 H_5^+$ and $H_5^0 H_5^-$ are shown in [13]. The fiducial cross section is constrained by the following expression:

$$\sigma_{fiducial} = (\sigma_{H_5^0 H_5^+} \times \epsilon_+ + \sigma_{H_5^0 H_5^-} \times \epsilon_-) \times \mathcal{B}(H_5^0 \rightarrow \gamma\gamma), \quad (32)$$

where the efficiencies ϵ_\pm for $H_5^0 H_5^\pm$ respectively, are shown in [13]. As we will see later, only the 8 TeV constraints are relevant to (32) since the 13 TeV cross section values are 3 orders of magnitude suppressed with respect to the experimental bounds.

The $b \rightarrow s$ transition bounds

Since the charged triplet H_3^\pm is partially coming from the SM doublet as shown in (8), then it couples to the up and down quarks similar to the way the W gauge boson does. These interactions lead to flavor violating processes such as the $b \rightarrow s$ transition ones, which depend only on the charged triplet mass m_3 and the mixing angle β . The current experimental value of the $b \rightarrow s\gamma$ branching ratio, for a photon energy $E_\gamma > 1.6 \text{ GeV}$ is $\mathcal{B}(\bar{B} \rightarrow X_s \gamma)_{exp} = (3.55 \pm 0.24 \pm 0.09) \times 10^{-4}$, while the two SM predictions are $\mathcal{B}(\bar{B} \rightarrow X_s \gamma)_{SM} = (3.15 \pm 0.23) \times 10^{-4}$ [34] and $\mathcal{B}(\bar{B} \rightarrow X_s \gamma)_{SM} = (2.98 \pm 0.26) \times 10^{-4}$ [35]. In our numerical scan, we consider the bounds on the m_3 - v_χ plan shown in [14].

V. NUMERICAL ANALYSIS AND DISCUSSION

We perform a numerical scan over the parameter space of the GM model and probe the effect of different theoretical and experimental constraints on the parameter space. We require the light CP – *even* scalar to be the 125 GeV SM-like Higgs boson and impose the constraints from perturbativity, unitarity, boundness from below, the diphoton Higgs decay, the Higgs total decay width, the Higgs signal strength modifiers, the electroweak precision tests, the constraints from the doubly charged Higgs bosons and Drell-Yan diphoton production, and the indirect constraint from the $b \rightarrow s\gamma$ transition processes.

We choose the model free parameters to be λ_2 , λ_4 , m_η , m_3 , m_5 , s_α and $s_\beta \equiv \sin \beta = 2\sqrt{2}v_\xi/v$, which lie in the ranges,

$$78 \text{ GeV} < m_3 < 1 \text{ TeV}, 78 \text{ GeV} < m_5 < 1.8 \text{ TeV}, m_h < m_\eta < 1 \text{ TeV}, |\lambda_{2,4}| \leq 10, |s_\beta| \leq 1, \quad (33)$$

where the triplet and fiveplet charged scalars are subject to a mass lower bound from LEP [21]. Here, the negative values of s_β should be considered due to the following reason. In the GM model, we have $V(\Phi, \Delta, \mu_{1,2}) = V(\Phi, -\Delta, -\mu_{1,2})$, and therefore all the mass matrix elements are also invariant under this transformation. However, since the scalar eigenstates are mixtures of the components of Φ and Δ , the physical vertices that involves scalars are not invariant under $(\Phi, \Delta, \mu_{1,2}) \rightarrow (\Phi, -\Delta, -\mu_{1,2})$. This means that any two BPs with the same input parameters but with opposite signs of $(\pm s_\beta, \pm \mu_{1,2})$ are physically different. This makes the negative s_β values in (33) independent parameter space that should not be ignored.

In order to check whether there exist wrong vacua that are deeper than the EW one $(v_\phi, \sqrt{2}v_\xi, v_\xi)$, we show in Fig. 2 the scalar mass ranges with (left) and without (right) the condition (15).

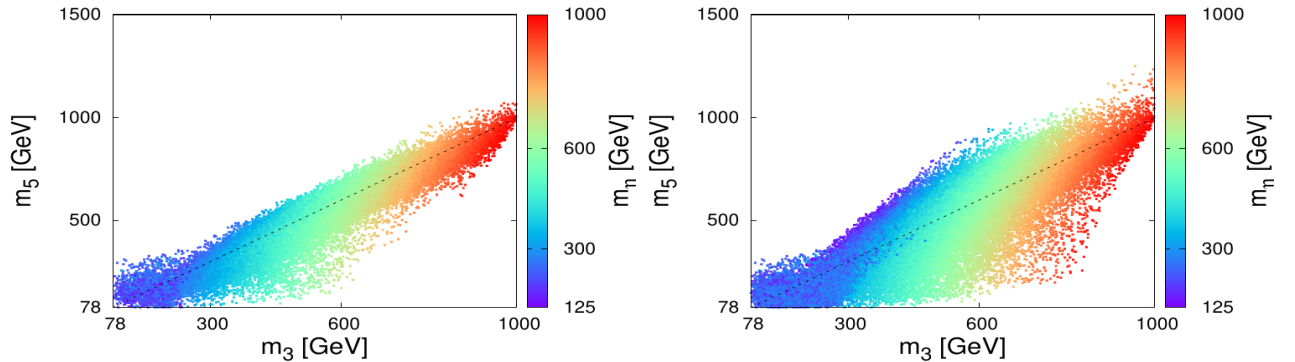


FIG. 2: The masses for triplet, fiveplet and singlet η estimated in the GM model by considering the basic theoretical and experimental constraints with (left) and without (right) the condition of the EW vacuum to be the deepest (15).

From the 58.5k BPs, 35k BPs fulfill the condition (15). This means that almost 40 % of the parameter space considered in the literature are excluded by the fact that the EW vacuum $(v_\phi, \sqrt{2}v_\xi, v_\xi)$ is not the deepest one. Clearly, when considering all the theoretical and experimental constraints except the condition (15), the fiveplet and the singlet η masses can reach the values $m_5 = 1.25 \text{ TeV}$ and $m_\eta = 1 \text{ TeV}$, respectively for the triplet maximal mass value $m_3 = 1 \text{ TeV}$. However, when considering the constraint (15), the fiveplet mass ranges get shrunk as $m_5 < 1.1 \text{ TeV}$. This requires a full reanalysis of different phenomenological aspects of this model. The viable parameter space in Fig. 2-right is a consequence of a combination of the theoretical and experimental constraints mentioned above.

In what follows, we will consider only the 35k viable BPs in our analysis, as shown in Fig. 3

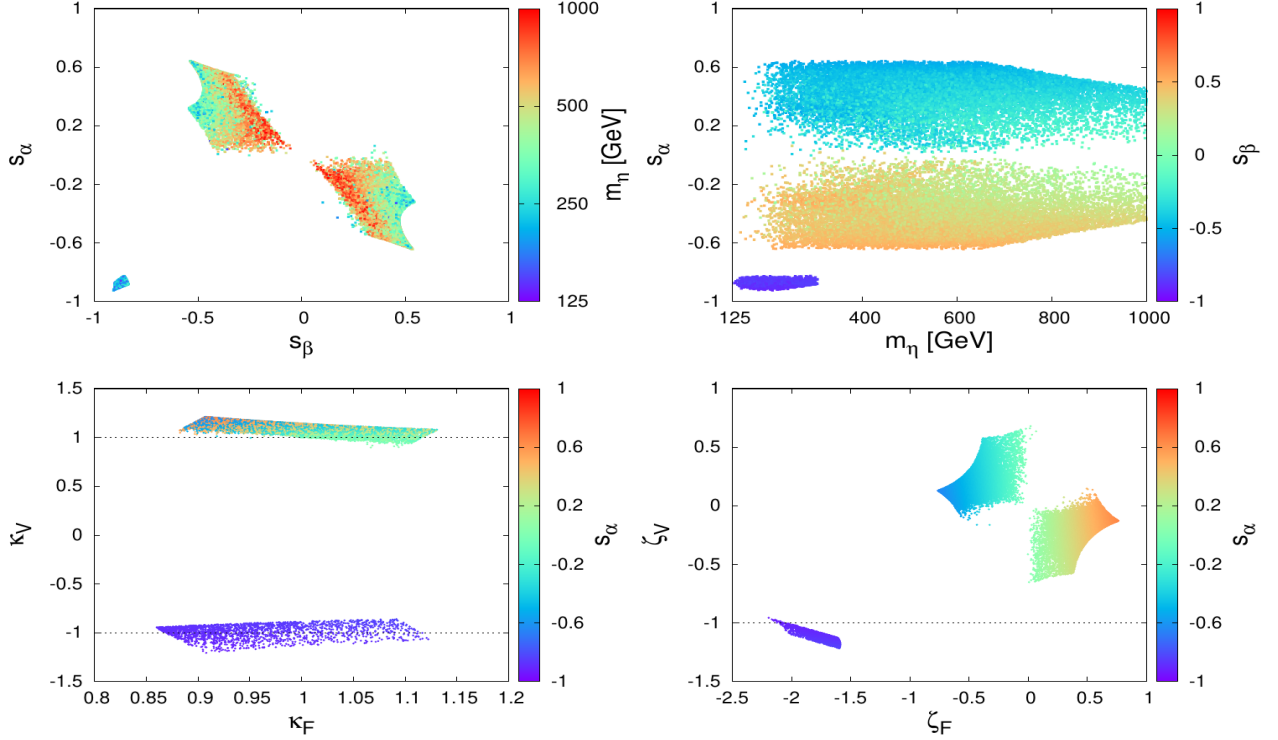


FIG. 3: Different physical observables estimated in the GM model by considering the theoretical and experimental constraints, i.e., the BPs used to produce Fig. 2-left.

From Fig. 3, one has to mention that the parameter space is well constrained and split into three isolated islands in the plans of $\{s_\beta, s_\alpha\}$, $\{s_\alpha, m_\eta\}$ and $\{\zeta_F, \zeta_V\}$; and into two islands in the plans of $\{\kappa_F, \kappa_V\}$. For instance, the three islands correspond to the ranges $\{-0.92 < s_\beta < -0.83, -0.92 < s_\alpha < -0.81\}$, $\{-0.54 < s_\beta < -0.05, 0.01 < s_\alpha < 0.64\}$ and $\{0.04 < s_\beta < 0.54, -0.64 < s_\alpha < 0.03\}$, respectively. According to the bottom-right panel in Fig. 3, the κ 's values for the two islands are $\{-1.21 < \kappa_V < -0.85, 0.86 < \kappa_F < 1.12\}$ and $\{0.9 < \kappa_V < 1.23, 0.88 < \kappa_F < 1.13\}$, respectively. While, the corresponding ζ 's ranges are $\{-1.22 < \zeta_V < -0.97, -2.15 < \zeta_F < -1.59\}$, $\{-0.09 < \zeta_V < 0.66, -0.75 < \zeta_F < -0.02\}$ and $\{-0.65 < \zeta_V < 0.14, 0.04 < \zeta_F < 0.75\}$, for the three islands, respectively. Here, the shape of all islands is dictated by the combination of all the above mentioned constraints, however, some of the constraints could have the dominant impact on such a region. For instance, the shape of the isolated islands is mainly dictated by the bounds from $b \rightarrow s$.

The Higgs coupling modifier κ_V is very constrained and could have both signs, while the κ_F deviation with respect to the SM can reach 13 %. These deviations of $\kappa_{F,V}$ from the SM are possible due to the strength of the bounds from some experimental constraints, such as the diphoton Higgs decay, the bounds on the total Higgs decay width and the Higgs signal strength modifiers. Unlike most of the SM extensions that involve a heavy scalar whose couplings to the fermions and gauge bosons are similar to those of the SM-like Higgs bosons, the scaling factor could have values larger than unity $|\zeta_F| > 1$. The reason of the significant deviation of the factors ζ_V, κ_V from unity, could be the factor $\sqrt{8/3}$, in addition to the sine and cosine in the denominator in (27) and (19). These values are very similar to the results obtained in [13] for

the region of positive κ_V due to the stringent constraints from the $b \rightarrow s$ transition bounds. However, we got another region with negative κ_V values that is not mentioned in [13], as it is allowed all the constraints considered in our scan of the full free parameters ranges (33).

In the majority of SM scalar extensions where the heavy scalar η couplings to the fermions and gauge bosons are much smaller than the SM values ($|\zeta_{F,V}| \ll 1$). This makes these models in agreement with all the negative searches of a heavy resonance. But in the GM model, the situation is different, i.e., $\zeta_{F,V}$ are not suppressed, and these negative searches could play a key role to exclude most of the parameter space as will be seen next.

In Fig. 4, we show the ratios $R_{\gamma\gamma}$ and $R_{\gamma Z}$ for the SM-like Higgs boson (left) and the Higgs total decay width versus its branching ratios (right).

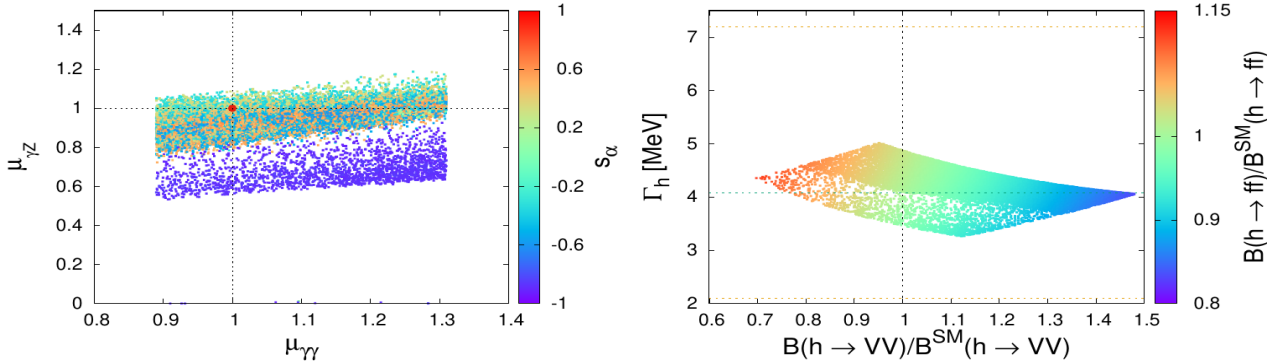


FIG. 4: Left: the ratio $R_{\gamma Z}$ in function of $R_{\gamma\gamma}$, where the palette shows the sine of the mixing angle α . Right: the SM-like Higgs total decay width versus Higgs branching ratio to gauge bosons scaled by its SM value. The palette shows the Higgs branching ratio to fermions scaled by its SM value; and the dashed line at $\Gamma_h = 4.08$ MeV corresponds to the SM value, while the experimentally allowed values are shown by the dashed lines at 2.1 MeV and 7.2 MeV [20].

From Fig. 4-left, while the values of $R_{\gamma\gamma}$ are constrained by the current LHC data [5], the ratio $R_{\gamma Z}$ is modified drastically with respect to the SM, it could be reduced by $\sim -45\%$ as it could be $\sim 18\%$ enhanced with respect to the SM. There are few BPs where $R_{\gamma Z}$ is almost null, which correspond to some specific values of $\kappa_{F,V}$, where a possible cancellation could occur between different terms in (26). From the right panel, one learns that the Higgs decays into gauge bosons and fermions can be reduced/enhanced by $-70 - 150\%$ and $-90 - 110\%$, respectively. Therefore, more precise Higgs measurements will tighten these ranges and constraint more the parameter space. For the considered parameter space, the oblique parameter given in (24) takes the values $-0.17 < \Delta S < 0.25$.

In Fig. 5, we present some observables relevant to the heavy scalar η versus its mass. In the left panel we show its total decay width and its invisible and undetermined branching fractions in the middle panel, while the SM branching ratios are shown in the right panel.

One has to mention that the singlet scalar η total decay width could be either 2 orders of magnitude smaller or larger than SM estimated value as shown in Fig. 5-left. This can be understood due the possible significant deviation of the factors $\zeta_{F,V}$ from unity, in addition to possible large values for the possible partial decay widths for $\eta \rightarrow hh, H_3H_3, H_5H_5$. According to Fig. 5-middle, one notices that the BSM channels could be dominant for $m_\eta > 160$ GeV. Here, one notes that the BSM branching ratios are dominant by

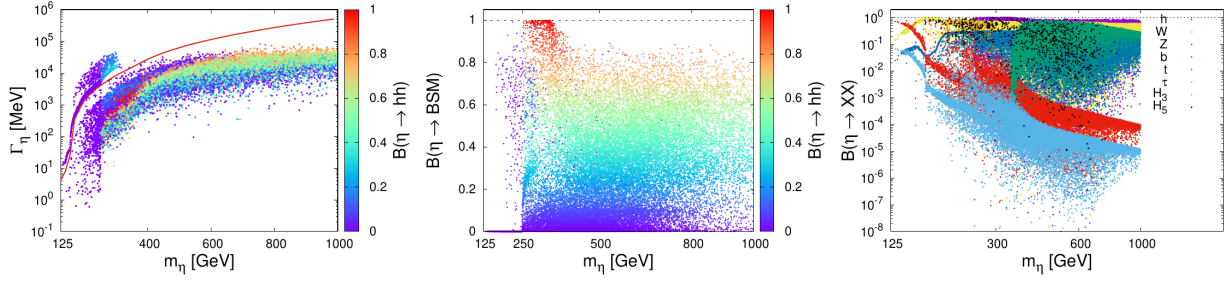


FIG. 5: Left: the total decay width of the scalar η in function of its mass m_η , where the palette shows its di-Higgs branching ratio. The red curve represents the total decay Γ_η estimated in the SM [23], i.e., with $s_\alpha = 1$ and $B_{BSM} = 0$. Middle: the BSM branching ratio $B_{BSM} = h, H_3, H_5$ versus m_η , where the palette shows the di-Higgs branching ratio. Right: the branching ratios $\mathcal{B}(\eta \rightarrow XX)$ versus m_η .

$\eta \rightarrow H_3 H_3$ and $\eta \rightarrow H_5 H_5$ in the region of mass $145 \text{ GeV} < m_\eta < 250 \text{ GeV}$ but when $m_\eta > 250 \text{ GeV}$ the BSM branching ratio is dominant by $\eta \rightarrow hh$. Clearly from Fig. 5-right, one remarks that the branching ratios $\mathcal{B}(\eta \rightarrow WW, ZZ, b\bar{b}, \tau\tau, tt)$ are comparable to their SM corresponding values [23] for a large portion of the BPs.

In Fig. 6, we show the resonant production cross section of the heavy scalar η compared to the experimental bounds in the channels $\tau\tau$ (left) and ZZ (right).

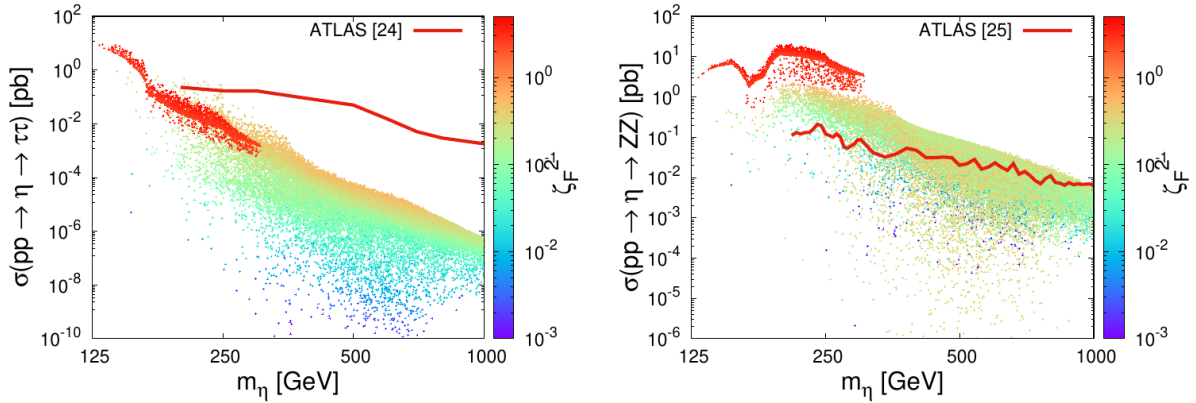


FIG. 6: The resonant production cross section $pp \rightarrow \eta \rightarrow \tau\tau$ (left) and $pp \rightarrow \eta \rightarrow ZZ$ (right) as a function of the heavy scalar mass m_η , where the palette shows the square of the scaling factor ζ_F . The red curves represent the corresponding experimental bounds from ATLAS [24, 25].

From Fig. 6, the experimental bounds from the negative searches for a heavy resonance in the channels $\tau\tau$ and ZZ exclude significant part of the parameter space. However, more regions in the parameter space will be excluded if the future searches for a heavy resonance would consider the mass range $125 - 200 \text{ GeV}$. For the $\eta \rightarrow ZZ$ constraint, if one extrapolates the bound into small m_η values, one learns that all the BPs with $\zeta_F^2 > 0.6$ are excluded.

Concerning the resonant production $\eta \rightarrow hh$, the production cross section can not be directly compared to the experimental bounds in the channels $hh \rightarrow b\bar{b}\tau\tau$ [28], $hh \rightarrow b\bar{b}b\bar{b}$ [29] and $hh \rightarrow b\bar{b}\gamma\gamma$ [30], since these analyses have been performed by taking into account the SM Higgs branching ratio. Therefore, the

modified cross section

$$\sigma^{mod}(pp \rightarrow \eta \rightarrow hh) = \sigma^{GM}(pp \rightarrow \eta \rightarrow hh) \times \frac{\mathcal{B}(h \rightarrow X_1 \bar{X}_1) \mathcal{B}(h \rightarrow X_2 \bar{X}_2)}{\mathcal{B}^{SM}(h \rightarrow X_1 \bar{X}_1) \mathcal{B}^{SM}(h \rightarrow X_2 \bar{X}_2)}, \quad (34)$$

is the relevant quantity to be compared with the experimental bounds [28–30] in the channel $hh \rightarrow X_1 \bar{X}_1 X_2 \bar{X}_2$. In Fig. 7, we show the modified cross section (34) as a function of the heavy scalar mass from the combination of $hh \rightarrow b\bar{b}\tau\tau$ and $hh \rightarrow b\bar{b}\gamma\gamma$ for the BPs with $m_\eta > 250$ GeV, where the palette shows the branching ratio of $\eta \rightarrow hh$.

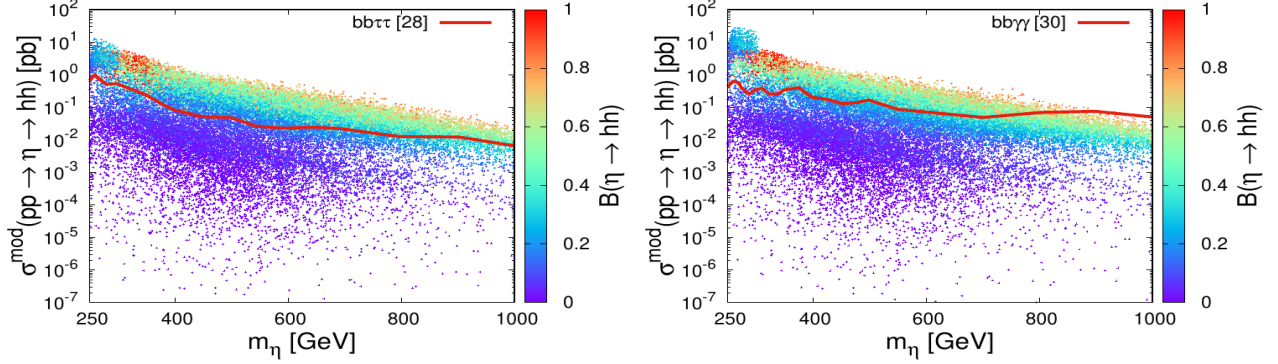


FIG. 7: The hh production cross section (34) as a function of m_η from the combination of $hh \rightarrow b\bar{b}\tau\tau$ [28], (left) and via $hh \rightarrow b\bar{b}\gamma\gamma$ [30] (right).

From Fig. 7, one learns that the majority of the BPs with $m_\eta > 250$ GeV are excluded by the experimental bounds [24–30]. One has to mention that the di-Higgs negative searches are used to set some limits on the triple Higgs couplings and to constrain the scalar sector in many multiscalar SM extensions, but here in the GM model, the resonant $\eta \rightarrow hh$ experimental bounds are very efficient in excluding large part of the parameter space. This point will be investigated in details in a future work [36].

Here, in Fig. 8 we show the effect of the constraints from the doubly charged Higgs bosons and Drell-Yan diphoton production on different observables like $s_\beta^2 \times \mathcal{B}(H_5^{++} \rightarrow W^+W^+)$ and the cross section of the diphoton production at 8 TeV which are plotted in function of m_5 and the corresponding branching ratio in the palette. One has to mention that it is worthless to show the cross section $pp \rightarrow H_5^0 \rightarrow \gamma\gamma$ at 13 TeV since the existing experimental bounds are given for the m_5 range [33], that it is already excluded by previous constraints.

One notices from Fig. 8-left that the branching ratio $\mathcal{B}(H_5^{++} \rightarrow W^+W^+)$ value does not play an important role in excluding the BPs by the experimental bounds [31]; however, the mixing value s_β does. From Fig. 8-right, one remarks that most of the diphoton scalar negative searches exclude most of the BPs with $\mathcal{B}(H_5^0 \rightarrow \gamma\gamma) > 0.09$, which is in good agreement with the experimental bound [32].

In Fig. 9, we reproduce the physical observables shown in Fig. 3 by considering only the BPs that are in agreement with all the above mentioned experimental bounds [24–30] fulfill the constraints from doubly charged Higgs boson and Drell-Yan diphoton production, the indirect constraints from the $b \rightarrow s$ transition processes and the LHC measurements on the Higgs strengths modifiers.

From the 35k BPs considered in our analysis, 74.5 % are excluded by the above combined constraints, where the majority of BPs correspond to $m_\eta < 2m_h$. However, most of them are not excluded due the

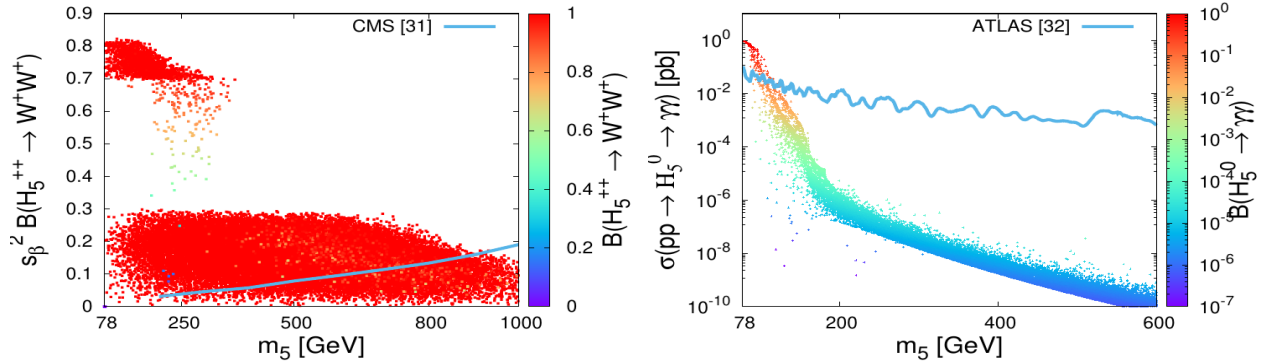


FIG. 8: Left: the quantity $s_\beta^2 \times \mathcal{B}(H_5^{++} \rightarrow W^+W^+)$ in function of m_5 , where the palette shows the branching ratio $\mathcal{B}(H_5^{++} \rightarrow W^+W^+)$. The blue curve represents the experimental bounds from CMS [31]. Right: the cross section of the diphoton production at 8 TeV, where the palette shows the corresponding branching ratio. The blue curve shows the experimental bound [32]. Here, the BPs with $m_5 > 600$ GeV are not considered since by the experimental bound [32] were established only for $m_5 < 600$ GeV.

absence of the experimental bounds for $m_5 < 200$ GeV. By comparing Fig. 9 with Fig. 3, one has to mention that these constraint do not change the shape of the islands described previously.

Before concluding this debate, it is essential to discuss the impact of future measurements at the HL-LHC on this model. The primary objectives of the HL-LHC include enhancing measurements related to the 125 GeV Higgs boson's couplings, decays, and the search for heavy Higgs particles. Additionally, it offers an important opportunity to test some BSM theories. In a study by Li [38], the possibility of observing the type-II seesaw doubly charged scalar was investigated. They obtained a mass upper bound of 655 GeV, which is irrelevant to the doubly charged scalar in the current model. According to the projections for Higgs property measurements [39], it is expected that the various Higgs scaling factors and, consequently, the signal strength modifiers in (22) will be measured with significantly improved precision. This will result in narrower experimentally allowed ranges for the scaling factors $\kappa_{F,V}$ as shown in (23), leading to the exclusion of a significant portion of the parameter space.

VI. CONCLUSION

In this work, we have studied the scalar potential of the GM model that preserves custodial SU(2) symmetry. We have considered the theoretical and experimental constraints on the parameter space such as the tree-level unitarity, the potential boundness from below, avoiding possibly deeper wrong minima, the electroweak precision tests, the Higgs total decay width and diphoton decay, and the Higgs strength modifiers, the negative searches on the doubly charged Higgs bosons and the Drell-Yan diphoton production, as well as the indirect constraints from the $b \rightarrow s$ transition processes; in addition to the direct searches for additional heavy Higgs resonances.

We performed a numerical scan based on all the above-mentioned theoretical and experimental constraints, and we found that the possible unwanted minima that could be deeper than the EW vacuum excludes about 40 % of the parameter space that fulfills the above mentioned constraints. On top of that, we noticed that the above constraints dictate a clear shape on the model parameter of three separated islands in the

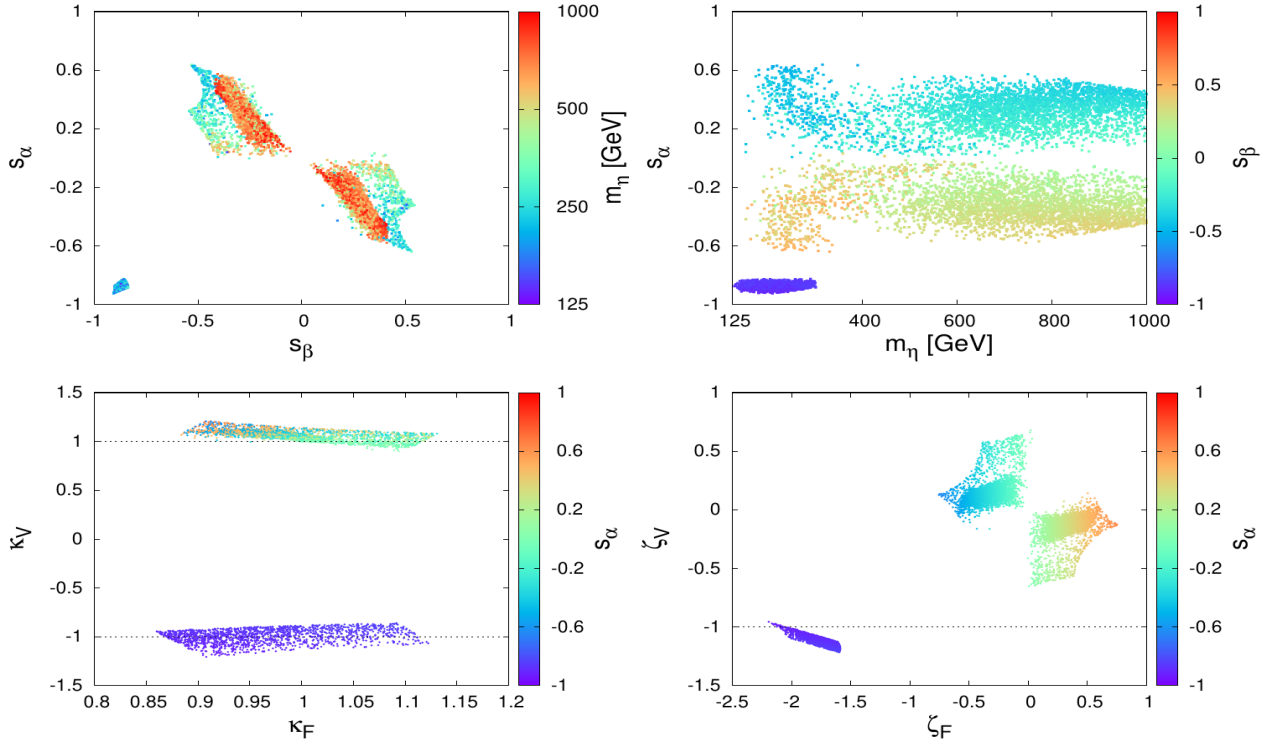


FIG. 9: The physical observables that are presented in Fig. 3 reproduced using only BPs that are in agreement with the recent ATLAS and CMS experimental bounds [24–30]; in addition to the constraints from the doubly charged Higgs bosons and Drell-Yan di-photon production [31–33] as well as the indirect constraints from $b \rightarrow s\gamma$ and the LHC measurements on the Higgs strengths modifiers.

plans of $\{s_\beta, s_\alpha\}$, $\{s_\alpha, m_\eta\}$ and $\{\zeta_F, \zeta_V\}$, and two islands in the plans of $\{\kappa_F, \kappa_V\}$. The couplings of the Higgs boson to the gauge bosons and fermions lie in the ranges $\{-1.21 < \kappa_V < -0.85, 0.86 < \kappa_F < 1.12\}$ and $\{0.9 < \kappa_V < 1.23, 0.88 < \kappa_F < 1.13\}$, respectively. However, the scaling factors of the heavy scalar η in the GM $\zeta_{F,V}$ lie in the ranges $\{-1.22 < \zeta_V < -0.97, -2.15 < \zeta_F < -1.59\}$, $\{-0.09 < \zeta_V < 0.66, -0.75 < \zeta_F < -0.02\}$ and $\{-0.65 < \zeta_V < 0.14, 0.04 < \zeta_F < 0.75\}$, respectively. Here, an isolated islands in the plans of that was supposed to exist was excluded by the $b \rightarrow s$ bound. The shape of the isolated islands as shown in the plans of $\{s_\beta, s_\alpha\}$, $\{s_\alpha, m_\eta\}$, $\{\zeta_F, \zeta_V\}$ and $\{\kappa_F, \kappa_V\}$ is dictated by the combination of the bounds of the Higgs signal strength modifiers and the Higgs total decay width; in addition to the Higgs diphoton decay.

We have also imposed the constraints from the negative searches of both doubly charged Higgs bosons in the VBF channel and Drell-Yan diphoton production, where we found that a significant part of the parameter space is excluded by the CMS bound on $s_\beta^2 \times \mathcal{B}(H_5^{++} \rightarrow W^+W^+)$ [31]. Here, it has been found that the branching ratio of $H_5^{++} \rightarrow W^+W^+$ does not play an important role in allowing/excluding any BP, but the mixing s_β does. Unfortunately, the recent bounds from CMS [31] and ATLAS [33] do not cover the mass range $m_5 < 200$ GeV, which makes a large part of the parameter space unconstrained by this severe bound. It will be interesting if future analyses would consider this mass range.

The indirect constraints from the $b \rightarrow s$ transition processes are also applied and put constraints on the two parameters m_3 and v_ξ only. We found also that the recent LHC measurements on the Higgs strengths modifiers impose strong constraints on the parameter space, especially the Higgs coupling modifiers $\kappa_{F,V}$.

In fact, the direct searches generally provide more strict constraints on the GM model parameter space and open the possibility of a discovery as these searches would be improved within the current/future LHC data. We have imposed also the recent ATLAS and CMS negative searches for the heavy scalar η in different channels. We found that the channel $\eta \rightarrow hh$ is very useful to exclude most of the parameter space, while, other channels are less efficient since the mass range $125 \text{ GeV} < m_\eta < 200 \text{ GeV}$ is not covered by most of the searches. Clearly, future searches and more precise measurements will tighten the parameter space of the GM model.

Appendix A: FUNCTIONS

The loop functions used in (24) are given by

$$\begin{aligned} f_1(x, y) &= \frac{5(y^6 - x^6) + 27(x^4y^2 - x^2y^4) + 12(x^6 - 3x^4y^2) \log x + 12(3x^2y^4 - y^6) \log y}{36(y^2 - x^2)^3}, \\ f_3(x, y) &= \frac{x^4 - y^4 + 2x^2y^2(\log y^2 - \log x^2)}{2(x^2 - y^2)^3}, \end{aligned} \quad (\text{A1})$$

while those used in (25) and (26) are given by [37]

$$\begin{aligned} A_1^{\gamma\gamma}(\tau) &= 2 + 3\tau + 3\tau(2 - \tau)f(\tau), \quad A_{1/2}^{\gamma\gamma}(\tau) = -2\tau[1 + (1 - \tau)f(\tau)], \quad A_0^{\gamma\gamma}(\tau) = \tau[1 - \tau f(\tau)], \\ A_1^{\gamma Z}(\tau, \lambda) &= -\cot\theta_W(4(3 - \tan^2\theta_W)I_2(\tau, \lambda) + [(1 + \frac{2}{\tau})\tan^2\theta_W - (5 + \frac{2}{\tau})]I_1(\tau, \lambda)), \\ A_{1/2}^{\gamma Z}(\tau, \lambda) &= I_1(\tau, \lambda) - I_2(\tau, \lambda), \quad A_0^{\gamma Z}(\tau, \lambda) = I_1(\tau, \lambda) \\ I_1(a, b) &= \frac{ab}{2(a-b)} + \frac{a^2b^2}{2(a-b)^2}[f(a) - f(b)] + \frac{a^2b}{(a-b)^2}[g(a) - g(b)], \\ I_2(a, b) &= -\frac{ab}{2(a-b)}[f(a) - f(b)], \end{aligned} \quad (\text{A2})$$

with

$$f(\tau) = \begin{cases} [\arcsin(\sqrt{\frac{1}{\tau}})]^2 & \text{if } \tau \geq 1, \\ -\frac{1}{4} \left[\log\left(\frac{1+\sqrt{1-\tau}}{1-\sqrt{1-\tau}}\right) - i\pi \right]^2 & \text{if } \tau < 1, \end{cases}, \quad g(\tau) = \begin{cases} \sqrt{\tau-1}[\sin^{-1}(\sqrt{\frac{1}{\tau}})] & \text{if } \tau \geq 1, \\ \frac{1}{2}\sqrt{\tau-1}[\log(\frac{\eta_+}{\eta_-}) - i\pi] & \text{if } \tau < 1. \end{cases} \quad (\text{A3})$$

Appendix B: COUPLINGS

Here, we give the couplings used in different observables definitions. The couplings that are used in (24) are

$$\begin{aligned} g_{ZhH_3^0} &= -i\sqrt{\frac{2}{3}}\frac{e}{s_Wc_W}(s_\alpha c_\beta + \sqrt{\frac{3}{8}}c_\alpha s_\beta), \quad g_{Z\eta H_3^0} = i\sqrt{\frac{2}{3}}\frac{e}{s_Wc_W}(c_\alpha c_\beta - \sqrt{\frac{3}{8}}s_\alpha s_\beta), \quad g_{ZH_3^0 H_3^0} = -i\sqrt{\frac{1}{3}}\frac{e}{s_Wc_W}c_\beta, \\ g_{ZZ\eta} &= \frac{e^2}{2s_W^2c_W^2}(s_\alpha c_\beta + \sqrt{\frac{8}{3}}c_\alpha s_\beta), \quad g_{ZZh} = \frac{e^2}{2s_W^2c_W^2}(c_\alpha c_\beta - \sqrt{\frac{8}{3}}s_\alpha s_\beta), \quad g_{ZH_5^+ H_3^-} = \frac{e}{2s_Wc_W}c_\beta, \\ g_{ZZH_3^0} &= -\frac{1}{\sqrt{3}}\frac{e^2}{s_W^2c_W^2}s_\beta v, \quad g_{ZW^+ H_5^-} = -\frac{e^2}{2s_W^2c_W^2}s_\beta v, \quad g_{ZZh}^{SM} = \frac{e^2}{2s_W^2c_W^2}v. \end{aligned} \quad (\text{B1})$$

Here, g_{ZZh}^{SM} is the SM coupling. The couplings $g_{hXX, \eta XX}$ used in (25), (26) and (28) are

$$\begin{aligned}
g_{hH_5^+H_5^-} &= g_{hH_5^+H_5^-} = -8\sqrt{3}(\lambda_3 + \lambda_4)v_\xi s_\alpha + (4\lambda_2 + \lambda_5)v_\phi c_\alpha - 2\sqrt{3}\mu_2 s_\alpha, \\
g_{hH_3^+H_3^-} &= -\frac{8}{\sqrt{3}}\left(\frac{\sqrt{2}}{4}\lambda_5 s_\beta c_\beta v_\phi + ((\lambda_3 + 3\lambda_4)v_\xi - \frac{3\mu_2}{4})c_\beta^2 + \frac{3}{2}(\lambda_2 + \frac{\lambda_5}{6})v_\xi + \frac{\mu_1}{24}s_\beta^2\right)s_\alpha \\
&\quad + 2\sqrt{2}c_\alpha c_\beta s_\beta (\lambda_5 v_\xi + \frac{\mu_1}{2}) + 4c_\alpha \left((\lambda_2 - \frac{\lambda_5}{4})c_\beta^2 + 2\lambda_1 s_\beta^2 v_\phi \right), \\
g_{\eta hh} &= -2\sqrt{3}c_\alpha \left((\lambda_5 - 2\lambda_2)v_\xi + \frac{\mu_1}{4} \right) c_\alpha^2 - 4s_\alpha^2 \left((\lambda_3 + 3\lambda_4 + \frac{\lambda_5}{2} - \lambda_2)v_\xi + \frac{\mu_1}{8} - \frac{\mu_2}{2} \right) \\
&\quad + 4s_\beta \left((\lambda_5 + 6\lambda_1 - 2\lambda_2)c_\alpha^2 - \frac{s_\alpha^2}{2}(\lambda_5 - 2\lambda_2) \right) v_\phi, \\
g_{\eta H_5^+H_5^-} &= g_{\eta H_5^+H_5^-} = g_{\eta H_5^0H_5^0} = 8\sqrt{3}(\lambda_3 + \lambda_4)v_\xi s_\alpha + (4\lambda_2 + \lambda_5)v_\phi c_\alpha + 2\sqrt{3}\mu_2 s_\alpha, \\
g_{\eta H_3^+H_3^-} &= g_{\eta H_3^0H_3^0} = \frac{8}{\sqrt{3}}\left(\frac{\sqrt{2}}{4}\lambda_5 c_\beta s_\beta v_\phi + ((\lambda_3 + 3\lambda_4)v_\xi - \frac{3\mu_2}{4})c_\beta^2 + \frac{3}{2}((\lambda_2 + \frac{\lambda_5}{6})v_\xi + \frac{\mu_1}{24})s_\beta^2\right)c_\alpha \\
&\quad + 2\sqrt{2}s_\alpha c_\beta s_\beta (\lambda_5 v_\xi + \frac{\mu_1}{2}) + 4s_\alpha \left((\lambda_2 - \frac{\lambda_5}{4})c_\beta^2 + 2\lambda_1 s_\beta^2 v_\phi \right), \tag{B2}
\end{aligned}$$

The coefficients C_{ZXX} used in (26) are given by

$$C_{ZH_5^+H_5^-} = \frac{1 - 2s_W^2}{s_W c_W}, \quad C_{ZH_3^+H_3^-} = C_{ZH_5^+H_5^-} = \frac{1 - 2s_W^2}{2s_W c_W}. \tag{B3}$$

Appendix C: WRONG MINIMA

The GM scalar potential may have other minima than the EW one. It is possible to get analytic formula for some these wrong minima, like the ones below, but others require numerical efforts. The following minima are possible only if the quantities inside the square-root are positive.

In the $CP - even$ subspace: we have eight possible minima that corresponds to V_i^{0+} ,

$$\begin{aligned}
\{h_\phi, h_\chi, h_\xi\} &= \left(\pm \frac{\sqrt{-\lambda_1 m_1^2}}{2\lambda_1}, 0, 0 \right), \left(0, \pm \frac{\sqrt{-2m_2^2(2\lambda_4 + \lambda_3)}}{2(2\lambda_4 + \lambda_3)}, 0 \right), \\
&\quad \left(0, 0, \pm \frac{\sqrt{-m_2^2(\lambda_4 + \lambda_3)}}{2(\lambda_4 + \lambda_3)} \right), \left(0, \frac{1}{\lambda_3} \sqrt{\frac{-m_2^2 \lambda_3^2 - 9\mu_2^2 \lambda_3 - 9\mu_2^2 \lambda_4}{2\lambda_3 + 4\lambda_4}}, -\frac{3\mu_2}{2\lambda_3} \right), \\
&\quad \left(0, \pm \frac{\sqrt{3\mu_2 \sqrt{-4m_2^2 \lambda_3 - 12m_2^2 \lambda_4 + 9\mu_2^2} - 2m_2^2 \lambda_3 - 6m_2^2 \lambda_4 + 9\mu_2^2}}{2\lambda_3 + 6\lambda_4}, \frac{3\mu_2 + \sqrt{-4m_2^2 \lambda_3 - 12m_2^2 \lambda_4 + 9\mu_2^2}}{4\lambda_3 + 12\lambda_4} \right), \\
&\quad \left(0, \pm \frac{\sqrt{-3\mu_2 \sqrt{-4m_2^2 \lambda_3 - 12m_2^2 \lambda_4 + 9\mu_2^2} - 2m_2^2 \lambda_3 - 6m_2^2 \lambda_4 + 9\mu_2^2}}{2\lambda_3 + 6\lambda_4}, \frac{3\mu_2 + \sqrt{-4m_2^2 \lambda_3 - 12m_2^2 \lambda_4 + 9\mu_2^2}}{4\lambda_3 + 12\lambda_4} \right), \\
&\quad \left(0, \pm \frac{\sqrt{3\mu_2 \sqrt{-4m_2^2 \lambda_3 - 12m_2^2 \lambda_4 + 9\mu_2^2} - 2m_2^2 \lambda_3 - 6m_2^2 \lambda_4 + 9\mu_2^2}}{2\lambda_3 + 6\lambda_4}, -\frac{-3\mu_2 + \sqrt{-4m_2^2 \lambda_3 - 12m_2^2 \lambda_4 + 9\mu_2^2}}{4\lambda_3 + 12\lambda_4} \right), \\
&\quad \left(0, \pm \frac{\sqrt{-3\mu_2 \sqrt{-4m_2^2 \lambda_3 - 12m_2^2 \lambda_4 + 9\mu_2^2} - 2m_2^2 \lambda_3 - 6m_2^2 \lambda_4 + 9\mu_2^2}}{2\lambda_3 + 6\lambda_4}, -\frac{-3\mu_2 + \sqrt{-4m_2^2 \lambda_3 - 12m_2^2 \lambda_4 + 9\mu_2^2}}{4\lambda_3 + 12\lambda_4} \right). \tag{C1}
\end{aligned}$$

In the $CP - odd$ subspace: we got three possible minima that corresponds to V_i^{0-} ,

$$\begin{aligned}
\{a_\phi, a_\chi\} &= \left(\pm \frac{\sqrt{-\lambda_1 m_1^2}}{2\lambda_1}, 0 \right), \left(0, \pm \frac{\sqrt{-2m_2^2(2\lambda_4 + \lambda_3)}}{2(2\lambda_4 + \lambda_3)} \right), \\
&\quad \left(\sqrt{\frac{-8m_1^2 \lambda_3 - 16m_1^2 \lambda_4 + 8m_2^2 \lambda_2 - 2m_2^2 \lambda_5}{32\lambda_1 \lambda_3 + 64\lambda_1 \lambda_4 - 16\lambda_2^2 + 8\lambda_2 \lambda_5 - \lambda_5^2}}, \sqrt{\frac{8m_1^2 \lambda_2 - 2m_1^2 \lambda_5 - 16m_2^2 \lambda_1}{32\lambda_1 \lambda_3 + 64\lambda_1 \lambda_4 - 16\lambda_2^2 + 8\lambda_2 \lambda_5 - \lambda_5^2}} \right). \tag{C2}
\end{aligned}$$

In the singly charged subspace: in this direction, we parametrized the charged fields as $X^\pm = |X|e^{\pm ie}$,

and then we found that the minima that correspond to V_i^\pm do not depend on the phases, i.e.,

$$\begin{aligned} \{|\phi^\pm|, |\chi^\pm|, |\xi^\pm|\} &= \left(\pm \frac{\sqrt{-2\lambda_1 m_1^2}}{4\lambda_1}, 0, 0 \right), \left(0, \pm \frac{\sqrt{-2m_2^2(\lambda_4 + \lambda_3)}}{4(\lambda_4 + \lambda_3)}, 0 \right), \left(0, 0, \pm \frac{\sqrt{-2m_2^2(\lambda_4 + \lambda_3)}}{4(\lambda_4 + \lambda_3)} \right), \\ &\left(\sqrt{\frac{\lambda_2 m_1^2 - 2\lambda_1 m_2^2}{16\lambda_1 \lambda_3 + 16\lambda_1 \lambda_4 - 4\lambda_2^2}}, \sqrt{\frac{-2\lambda_3 m_1^2 - 2\lambda_4 m_1^2 + \lambda_2 m_2^2}{16\lambda_1 \lambda_3 + 16\lambda_1 \lambda_4 - 4\lambda_2^2}}, 0 \right), \left(\sqrt{\frac{-m_2^2}{16\lambda_4 + 8\lambda_3}}, 0, \sqrt{\frac{-m_2^2}{16\lambda_4 + 8\lambda_3}} \right), \\ &\left(0, \sqrt{\frac{-2\lambda_3 m_1^2 - 2\lambda_4 m_1^2 + \lambda_2 m_2^2}{16\lambda_1 \lambda_3 + 16\lambda_1 \lambda_4 - 4\lambda_2^2}}, \sqrt{\frac{\lambda_2 m_1^2 - 2\lambda_1 m_2^2}{16\lambda_1 \lambda_3 + 16\lambda_1 \lambda_4 - 4\lambda_2^2}} \right). \end{aligned} \quad (C3)$$

In the doubly charged subspace: in the doubly charged directions we have only one possible minimum, which is given by

$$|\chi^{\pm\pm}| = \frac{\sqrt{-m_2^2(2\lambda_4 + \lambda_3)}}{2(2\lambda_4 + \lambda_3)}. \quad (C4)$$

Acknowledgements: We would like to thank Abdesslam Arhrib for his valuable comments. The work of A.A. is funded by the University of Sharjah under the Research Projects No. 21021430107 “*Hunting for New Physics at Colliders*” and No. 23021430135 “*Terascale Physics: Colliders vs Cosmology*”.

-
- [1] G. Aad et al. (ATLAS Collaboration), Phys. Lett. B **716**, 1 (2012);
S. Chatrchyan et al. (CMS Collaboration), Phys. Lett. B **716** 30 (2012).
- [2] G. Bertone, D. Hooper, and J. Silk, Phys. Rep. **405**, 279 (2005).
- [3] Y. Fukuda et al. (Super-Kamiokande Collaboration), Phys. Rev. Lett. **81**, 1562 (1998).
- [4] H. Georgi and M. Machacek, Nucl. Phys. **B262**, 463 (1985).
- [5] R. L. Workman et al. (Particle Data Group), Prog. Theor. Exp. Phys. **2022**, 083C01 (2022).
- [6] A. Ahriche, Phys. Rev. D **107**, 015006 (2023).
- [7] C. W. Chiang, A. L. Kuo, and K. Yagyu, J. High Energy Phys. 10 (2013) 072.
- [8] M. S. Chanowitz and M. Golden, Phys. Lett. **165B**, 105 (1985); J. F. Gunion, R. Vega, and J. Wudka, H. E. Haber and H. E. Logan, Phys. Rev. D **62**, 015011 (2000); M. Aoki and S. Kanemura, Phys. Rev. D **77**, 095009 (2008); **89**, 059902(E) (2014); S. Godfrey and K. Moats, Phys. Rev. D **81**, 075026 (2010); I. Low and J. Lykken, J. High Energy Phys. 10, (2010) 053; H. E. Logan and M. A. Roy, Rev. D **82**, 115011 (2010); S. Chang, C. A. Newby, N. Raj, and C. Wanotayaroj, Phys. Rev. D **86**, 095015 (2012); S. Kanemura, M. Kikuchi, and K. Yagyu, Phys. Rev. D **88**, 015020 (2013); C. Englert, E. Re, and M. Spannowsky, Rev. D **87**, 095014 (2013); R. Killick, K. Kumar, and H. E. Logan, Phys. Rev. D **88**, 033015 (2013); C. Englert, E. Re, and M. Spannowsky, 035024 (2013); C. W. Chiang, arXiv:1504.06424; C. Degrande, K. Hartling, and H. E. Logan, Phys. Rev. D **96**, 075013 (2017); **98**, 019901(E) (2018); N. Ghosh, S. Ghosh, and I. Saha, Phys. Rev. D **101**, 015029 (2020); D. Das and I. Saha, Phys. Rev. D **98** 095010 (2018); A. Ismail, B. Keeshan, H. E. Logan, and Y. Wu, Phys. Rev. D **103**, 095010 (2021); A. Ismail, H. E. Logan, and Y. Wu, arXiv:2003.02272; C. Wang, J. Q. Tao, M. A. Shahzad, G. M. Chen, and S. Gascon-Shotkin, arXiv:2204.09198; A. Ismail, B. Keeshan, H. E. Logan, and Y. Wu, Phys. Rev. D **103**, 095010; A. Adhikary, N. Chakrabarty, I. Chakraborty, and J. Lahiri, Eur. Phys. J. C **816**, 554 (2021).
- [9] K. Hartling, K. Kumar, and H. E. Logan, Phys. Rev. D **90**, 015007 (2014).
- [10] S. L. Chen, A. Dutta Banik, and Z. K. Liu, Nucl. Phys. **B966**, 115394 (2021).
- [11] T. Pilkington, arXiv:1711.04378.
- [12] C. W. Chiang and T. Yamada, Phys. Lett. B **735**, 295 (2014); R. Zhou, W. Cheng, X. Deng, L. Bian, and Y. Wu, J. High Energy Phys. **01** (2019) 216; T. K. Chen, C. W. Chiang, C. T. Huang, and B. Q. Lu, arXiv:2205.02064.
- [13] A. Ismail, H. E. Logan, and Y. Wu, arXiv:2003.02272.

- [14] K. Hartling, K. Kumar, and H. E. Logan, *Phys. Rev. D* **91**, 015113 (2015).
- [15] C. W. Chiang, G. Cottin, and O. Eberhardt, *Phys. Rev. D* **99**, 015001 (2019).
- [16] G. Moulataka and M. C. Peyranre, *Phys. Rev. D* **103**, 115006 (2021).
- [17] J. Baron *et al.* (ACME Collaboration), *Science* **343**, 269 (2014).
- [18] D. Azevedo, P. Ferreira, H. E. Logan, and R. Santos, *J. High Energy Phys* **03** (2021) 221.
- [19] A. Arhrib, R. Benbrik, M. Chabab, G. Moulataka, M. C. Peyranere, L. Rahili and J. Ramadan, *Phys. Rev. D* **84**, 095005 (2011).
- [20] Evidence of off-shell Higgs boson production and constraints on the total width of the Higgs boson in the $ZZ \rightarrow 4\ell$ and $ZZ \rightarrow 2\ell 2\nu$ decay channels with the ATLAS detector, Report No. ATLAS-CONF-2022-068.
- [21] G. Abbiendi *et al.* (ALEPH, DELPHI, L3, OPAL and LEP Collaborations), *Eur. Phys. J. C* **73**, 2463 (2013).
- [22] M. Baak *et al.* (Gfitter Group), *Eur. Phys. J. C* **74**, 3046 (2014).
- [23] <https://twiki.cern.ch/twiki/bin/view/LHCPhysics/LHCHWG>.
- [24] G. Aad *et al.* (ATLAS Collaboration), *Phys Rev. Lett.* **125**, 051801 (2020).
- [25] G. Aad *et al.* (ATLAS Collaboration), *Eur. Phys. J. C* **81**, 332 (2021).
- [26] A. Tumasyan *et al.* (CMS Collaboration), *Phys. Rev. D* **105**, 032008 (2022).
- [27] (ATLAS Collaboration), Summary of non-resonant and resonant Higgs boson pair searches from the ATLAS experiment, Report No. ATL-PHYS-PUB-2021-031.
- [28] ATLAS Collaboration, Search for resonant and non-resonant Higgs boson pair production in the $b\bar{b}\tau^+\tau^-$ decay channel using 13 TeV pp collision data from the ATLAS detector, Report No. ATLAS-CONF-2021-030.
- [29] ATLAS Collaboration, Search for resonant pair production of Higgs bosons in the $b\bar{b}b\bar{b}$ final state using pp collisions at $\sqrt{s} = 13$ TeV with the ATLAS detector, Report No. ATLAS-CONF-2021-035.
- [30] ATLAS Collaboration, Search for Higgs boson pair production in the two bottom quarks plus two photons final state in pp collisions at $\sqrt{s} = 13$ TeV with the ATLAS detector, Report No. ATLAS-CONF-2021-016.
- [31] A. M. Sirunyan *et al.* (CMS Collaboration), *Phys. Rev. Lett.* **120**, 081801 (2018).
- [32] G. Aad *et al.* (ATLAS Collaboration), *Phys. Rev. Lett.* **113**, 171801 (2014).
- [33] M. Aaboud *et al.* (ATLAS Collaboration), *Phys. Lett. B* **775**, 105 (2017).
- [34] M. Misiak, H. M. Asatrian, K. Bieri, M. Czakon, A. Czarnecki, T. Ewerth, A. Ferroglia, P. Gambino, M. Gorbahn, C. Greub, *et al.*, *Phys. Rev. Lett.* **98**, 022002 (2007).
- [35] T. Becher and M. Neubert, *Phys. Rev. Lett.* **98**, 022003 (2007).
- [36] A. Ahriche, *The Di-Higgs Production at the LHC in the Georgi-Machacek Model*, (to be published).
- [37] A. Djouadi, *Phys. Rept.* **459**, 1 (2008).
- [38] T. Li, *J. High Energy Phys.* 09 (2018), 079.
- [39] Projections for measurements of Higgs boson signal strengths and coupling parameters with the ATLAS detector at a HL-LHC, Report No. ATL-PHYS-PUB-2014-016.